Research Article
doi.org/10.1002/ansa.202300057
Chemistry Europe
European Chemical Societies Publishing

Received: 11 November 2023
Accepted: 17 November 2023

A Raman spectral marker for the iso-octyl chain structure of cholesterol

Mathieu L. Simeral[1] | Steven M. E. Demers[1] | Kyle Sheth[1] | Jason H. Hafner[1,2]

[1]Department of Physics and Astronomy, Rice University, Houston, Texas, USA

[2]Department of Chemistry, Rice University, Houston, Texas, USA

Correspondence
Jason H. Hafner, Department of Physics and Astronomy, Rice University, Houston, TX 77005, USA.
Email: hafner@rice.edu

Funding information
National Science Foundation, Grant/Award Number: 1709084; Welch Foundation, Grant/Award Number: C-2140-20230405; United States Department of Defense, Office of the Assistant Secretary of Defense for Health Affairs and the Defense Health Agency J9, Research and Development Directorate, through the Peer Reviewed Medical Research Program Discovery Award, Grant/Award Number: W81XWH-21-1-0002

Abstract

Raman spectroscopy provides label-free, specific analysis of biomolecular structure and interactions. It could have a greater impact with improved characterization of complex fingerprint vibrations. Many Raman peaks have been assigned to cholesterol, for example, but the molecular vibrations associated with those peaks are not known. In this report, time-dependent density functional theory calculations of the Raman spectrum of cholesterol are compared to measurements on microcrystalline powder to identify 23 peaks in the Raman spectrum. Among them, a band of six peaks is found to be sensitive to the conformational structure of cholesterol's iso-octyl chain. Calculations on 10 conformers in this spectral band are fit to experimental spectra to probe the cholesterol chain structure in purified powder and in phospholipid vesicles. In vesicles, the chain is found to bend perpendicular to the steroid rings, supporting the case that the chain is a dynamic structure that contributes to lipid condensation and other effects of cholesterol in biomembranes.

Statement of Significance: Here we use density functional theory to identify a band of six peaks in cholesterol's Raman spectrum that is sensitive to the conformational structure of cholesterol's chain. Raman spectra were analyzed to show that in fluid-phase lipid membranes, about half of the cholesterol chains point perpendicular to the steroid rings. This new method of label-free structural analysis could make significant contributions to our understanding of cholesterol's critical role in biomembrane structure and function. More broadly, the results show that computational quantum chemistry Raman spectroscopy can make significant new contributions to molecular structure when spectra are interpreted with computational quantum chemistry.

1 | INTRODUCTION

Raman spectroscopy detects the molecular vibrations of substances from simple laser light scattering measurements.[1] It is a label-free analytical method that requires essentially no sample preparation while it provides molecular specificity associated with molecular vibrations. As Raman instrumentation has become more accessible, interest has grown in many fields, such as pharmaceuticals, mineralogy, astrobiology, archaeology and food science, to name only a few.[2–9] Biomedical applications are particularly promising due to the potential for label-free diagnostics and real-time intraoperative detection.[10–14] Lipids are a common target of Raman analysis due to their high concentration in biological samples, their variations with disease states and the unique molecular vibrations of their fatty acid chains.[15–17] For example, the purity and heterogeneity of exosomes have been studied by Raman spectroscopy, as well as the lipid components of bone marrow.[11,18–20]

This is an open access article under the terms of the Creative Commons Attribution-NonCommercial License, which permits use, distribution and reproduction in any medium, provided the original work is properly cited and is not used for commercial purposes.
© 2023 The Authors. *Analytical Science Advances* published by Wiley-VCH GmbH.

Research Article
doi.org/10.1002/ansa.202300057
Chemistry Europe
European Chemical Societies Publishing

Raman microscopy has tracked reservoirs of lipids within cells to reveal insights that are lost when samples are homogenized.[21–24] Biophysical studies of model membranes also benefit from Raman imaging, where molecular details can be seen without the need for probes that likely perturb the membrane structure.[25–28] Among lipids targets for Raman analysis, cholesterol is of particular interest given its prevalence in membranes and its fundamental role in membrane structure and cell biology.[29–33] Intracellular monitoring of cholesterol biosynthesis by Raman imaging can evaluate chemotherapy response in bladder cancer, as well as monitor lipid levels in liver disease and atherosclerosis.[14,21,34–36] In addition to living matter, cholesteroids are studied as molecular fossils in paleobiology that provide clues to dietary relationships in past ecosystems.[37]

Imprecise identification of the molecular vibrations associated with Raman peaks lessens the impact the spectra may have on deciphering molecular structure and interactions. Spectra of molecular analogues and isotopes help identify vibrations, but these methods are not effective beyond a certain molecular size and complexity. Density functional theory (DFT) calculations can fill this gap.[38] A molecule's normal mode vibrations can be calculated from the energy gradients of a DFT-optimized molecular structure. A subsequent calculation of changes in the molecular polarizability with each normal mode's motion produces the Raman spectrum. With well-chosen exchange-correlation potentials, basis sets and sufficient numerical precision, accurate spectra can be calculated for medium to large molecules (up to ~100 atoms).[39] The accuracy strongly depends on the molecular size and electronic properties, possible effects of resonance and surface enhancement and the details of the DFT calculation methodology.[40–44] For example, it has been shown that the calculation of time-dependent polarizabilities by time-dependent DFT (TDDFT) improved the accuracy of calculated Raman mode intensities for diatomic molecules.[45]

We have recently reported TDDFT calculated Raman spectra for anthraquinones and flavonoids and found good agreement with measured spectra since these fused-ring structures are not subject to significant conformational variation.[46,47] These studies also showed distinct signatures of hydrogen bonding in specific bands of the spectrum. Here we investigate cholesterol through comparisons of TDDFT calculated Raman spectra to measurements on microcrystalline powder and solution phase lipid vesicles. In addition to identifying Raman active vibrations, spectral markers for the molecular conformation of the iso-octyl chain are characterized.

2 | MATERIALS AND METHODS

2.1 | Lipid sample preparation

Powdered cholesterol (> 99% purity) was purchased from Sigma. 1,2-dioleoyl-sn-glycero-3-phosphocholine (DOPC) (> 99% purity) was purchased from Avanti Polar Lipids dissolved in chloroform. Both phospholipid-cholesterol (with a 3:1 molar ratio of phospholipids to cholesterol) and pure phospholipid solutions were prepared. The lipids were mixed in chloroform then the solution was dried under gentle argon flow for ~45 min and placed in a vacuum chamber for ~2 h until the pressure dropped below 1×10^{-5} Torr. The dried lipids were hydrated with deionized water to obtain a 10 mg/mL phospholipid concentration. The aqueous solutions were mixed and sonicated for ~20 min. First, mixing removed the lipids from the glass container wall forming a milky white multilamellar vesicle (MLV) solution. Secondly, sonication transformed the MLVs into small unilamellar vesicles turning the solution optically clear with a bluish tint. Vesicle solutions were stored in a refrigerator and used for measurements within 2 days.

2.2 | Raman spectroscopy

Raman spectra were recorded with a custom micro-Raman spectrometer. Excitation was provided by an Ondax RO-785 785 nm, 80 mW stabilized CW diode laser with beam power set by a Thorlabs NDL-25C-2 continuously variable neutral density filter. A Semrock LPD02-785RU-25 × 34 × 1.1 dichroic mirror directed the beam to an LCPLN100XIR near-infrared corrected 100x/0.85 NA microscope objective which then focused it onto the sample. Back-scattered light passed back through the objective, dichroic mirror and a Chroma RE792lp blocking filter. An Olympus LMPLN5XIR 5x/0.1 NA near-infrared corrected objective focused the filtered light onto the entrance slit of a Princeton Instruments IsoPlan SCT320 spectrograph. Spectra were recorded on a Princeton Instruments Pixis 256E thermoelectrically cooled, open-electrode CCD camera at a resolution of 6 cm^{-1}.

The cholesterol powder spectrum was obtained by applying a few mg to a support using double-sided carbon tape. Four images were obtained for four spectral regions centred at 810, 840, 870 and 900 nm using 20 min integrations and 20 mW laser power. The image pixel counts were summed vertically to obtain an intensity spectrum.

For the vesicle solution spectra, an LCPLN20XIR near-infrared corrected 20x/0.45 NA microscope objective was focused in a 1 × 1 mm borosilicate capillary tube (0.2 mm wall width). A custom-built system pumped the solution through the capillary to ensure the solution remained homogeneous throughout the measurement. The incident power was increased to 60 mW. Three images with 20 min integration time were averaged for the 840, 870 and 900 nm spectral regions. To reduce noise in the spectrum, the number of images was increased to 15 for the 810 nm spectral region. Finally, the phospholipid solution spectrum was subtracted from the phospholipid-cholesterol solution spectrum to obtain a vesicle Raman spectrum for cholesterol. Cholesterol alters the structure of phospholipid membranes, so it may also alter the phospholipid Raman spectrum, making it an inaccurate reference for subtraction. Fortunately, phospholipids have no strong Raman peaks in the region of interest (520–650 cm^{-1}).

2.3 | Time-dependent density functional theory

TDDFT calculations were carried out with the Amsterdam Density Functional program from Software for Chemistry & Materials (ADF 2019.306, SCM, Theoretical Chemistry; Vrije Universiteit).[38,48]

Research Article
doi.org/10.1002/ansa.202300057
Chemistry Europe
European Chemical Societies Publishing

Conformers were generated by the RDKit algorithm and then optimized by DFT. The calculation was performed with the following parameters: a Becke-Perdew exchange–correlation potential under the generalized gradient approximation with a third-order dispersion correction and Becke-Johnson damping (GGA/BP86-D3(BJ)), a quad zeta basis set with four polarization functions, no frozen core, no relativistic correction and good numerical quality.[49–52] Once the structure has been optimized, calculations of the second derivatives of the energy with respect to nuclear displacements yield the normal mode frequencies of each conformer. Finally, a Raman range calculation of time-dependent polarizabilities produced a theoretical Raman spectrum at an excitation frequency of 1.58 eV (785 nm) and a two-point numerical differentiation of the polarizability tensor.[45,50,53–57] The atomic coordinates and vibration amplitudes were imported into MATLAB software to create illustrations of the conformer structure and the molecular vibration maps. Mathematical details of the vibration map illustrations were described previously.[46]

2.4 | Spectral fitting

The experimental spectra were fit to a linear combination of the four spectral types by linear regression using MATLAB's Statistics and Machine Learning toolbox. The spectrum for each type was calculated as a thermally weighted average of the spectra of two or three conformers of that type. The experimental spectra were normalized and offset to have a minimum of zero in the spectral band. A 1.5% scale factor was applied to the frequencies of the calculated bands. The fit had only four coefficients (one for each spectral type) and no other free parameters. If unconstrained, the solution had a negative coefficient for type D_{2b}. We therefore applied the constraint that all coefficients be positive, which gave the results in Table 2 and caused the coefficient for D_{2b} to be zero. To find the confidence intervals, the fit was run unconstrained but without D_{2b}, which resulted in the same coefficients. The coefficients and confidence intervals in Table 2 were normalized for convenient comparisons.

3 | RESULTS AND DISCUSSION

3.1 | Identifying Raman modes in purified cholesterol

The earliest Raman investigations on cholesterol studied its impact on phospholipid acyl chain structure in lipid membranes. Spectral bands at 1672 and 600 cm^{-1} were assigned to cholesterol and used to estimate its relative concentration in membranes.[58,59] Faiman first reported the Raman spectrum of purified crystalline cholesterol.[60] Approximately 50 peaks were assigned to cholesterol, but most were deemed too complex to pursue. The methylene deformations between 1400 and 1500 cm^{-1} and C—H modes between 2700 and 3100 cm^{-1} were found to depend on its chain packing as they do for phospholipids. Continued investigations over the years have identified these and other vibrations

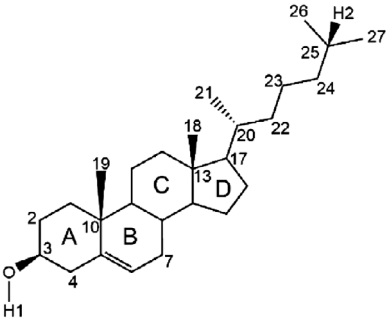

FIGURE 1 The cholesterol structure with relevant atom numbers and ring labels.

of cholesterol.[9,16] The peak at 1672 cm^{-1} is the C=C stretch in the ring structure, and peaks at 1087, 1130 and 1178 cm^{-1} are C—C and C—H vibrations. There are many vibrations below 1000 cm^{-1} whose molecular motions are ambiguous. Among these, peaks at 701, 604, 548 and 424 cm^{-1} are the strongest and are often associated with cholesterol.[16,61–64]

For accurate TDDFT spectral calculations, the molecular conformation must be considered since it affects molecular vibrations. We have found that conformational variation has a greater effect on the Raman spectra of flexible alkane chains than fused rings.[46,65] However, even for fused ring molecules like hydroxyanthraquinones, the orientation of individual hydroxyl groups affects the Raman peaks. For this study, cholesterol conformers were generated with RDKit software, which applies dihedral angles to rotatable bonds based on statistics from structural databases, and then carries out low-level energy calculations and structural refinement.[66] DFT refinement was then applied, which caused some conformers to converge to the same structure. Here spectral calculations of 10 unique conformers found by this process are reported. Vibrations and dihedral angles are defined following the standard atom numbers and ring labels shown in Figure 1.

Figure 2 displays calculated and experimental Raman spectra of cholesterol in two spectral windows. The calculated spectrum is sufficiently accurate that 23 peaks were identified based on their spacing and relative intensities. The low-frequency band in Figure 2A contains fingerprint vibrations of the fused ring structure. The higher band in Figure 2B contains well-known functional group peaks. The peaks between these bands (plotted in the Supporting Information) are too dense to make definitive assignments. Note that the calculated peak frequencies in Figure 2 have not been scaled.[67,68] Although they are off by approximately 1.5%, the spacing and amplitudes of the peaks are sufficiently accurate that assignments can be made without precisely matched peak positions.

At the lowest frequencies (peaks 1-9) the vibrations are distributed throughout the molecular structure. Moving to higher frequencies, peaks 10-18 are somewhat more localized skeletal vibrations of the chain, rings, methyl groups and hydroxyl group. Peaks 19-22 are methyl and methylene vibrations and peak 23 is the C=C stretch. As a way to visualize these complex vibrations with a static image, the structures are drawn with a bond width that represents its stretch amplitude and

Research Article
doi.org/10.1002/ansa.202300057
Chemistry Europe
European Chemical Societies Publishing

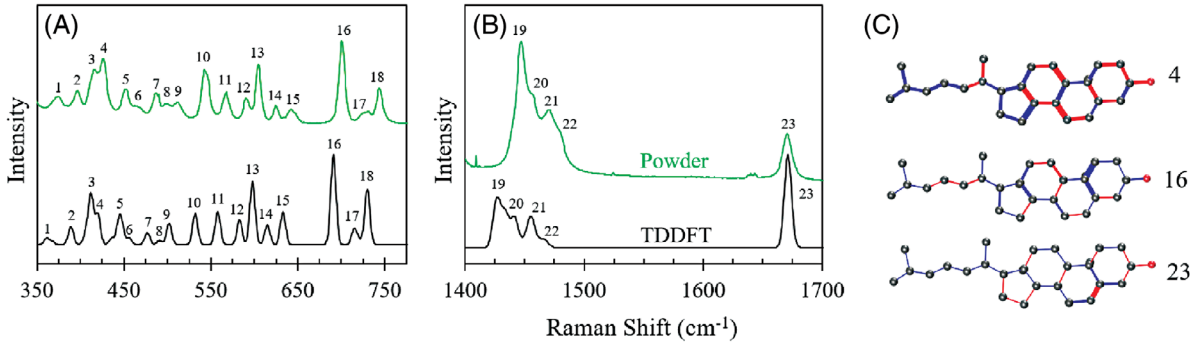

FIGURE 2 The Raman spectrum of cholesterol. The calculated (black) and experimental (green) spectra with labelled peaks match based on spacing and relative amplitude for low-frequency (A) and high-frequency (B) vibrations. Vibration maps are displayed for three of the peaks (C). The calculated spectra displayed are for conformer #1 in Table 1.

a red/blue colour to represent the relative phase.[46] Three such vibration maps are displayed in Figure 2C that illustrate a localized vibration (peak 23), a distributed vibration (peak 4) and the vibration for peak 16 that is most often used as a marker for cholesterol. The vibration maps for all 23 peaks can be found in the Supporting Material. The maps are useful for finding vibrations common to a molecular family, and for comparing modes of different conformers. Note that these maps only illustrate bond stretching, so they do not contain all vibrational information. The methyl and methylene vibrations of peaks 19–22, for example, are not well represented by such illustrations. Also, the maps do not indicate how much each stretching motion contributes to the Raman intensity for that mode.

TABLE 1 Torsion angles and relative total bonding energy of 10 cholesterol conformers, arranged by conformer type.

Conf	Type	ω_0	ω_1	ω_2	ω_3	ω_4	ω_5	ω_6	ω_7	E (kcal/mol)
1	A	182	180	190	176	176	187	63	−56	0.27
2	A	182	180	192	178	185	−63	173	56	0.30
3	A	57	180	191	176	176	187	63	−56	0.40
4	$D_{1,3}$	−62	176	62	174	60	182	58	−61	0.06
5	$D_{1,3}$	57	176	62	175	61	182	58	−61	0.07
6	$D_{1,3}$	163	174	63	183	−63	−57	179	62	0.18
7	D_{2a}	180	176	61	179	183	−63	174	56	0.00
8	D_{2a}	−62	176	61	178	175	187	63	−56	0.14
9	D_{2b}	180	176	61	178	179	63	−63	180	0.62
10	D_{2b}	−61	174	61	176	179	63	−63	180	0.72

3.2 | Raman spectra of different conformers of cholesterol

A comprehensive study of dozens of membrane sterol crystal structures by Duax et al. provides insight into the observed conformations of cholesterol.[69] Among the structures, the tetracyclic rings show little variation apart from some twisting around the five-membered ring. The iso-octyl chain conformation is determined by six dihedral angles defined by Duax et al. as:

$$\omega_1 = C13 - C17 - C20 - C22$$
$$\omega_2 = C17 - C20 - C22 - C23$$
$$\omega_3 = C20 - C22 - C23 - C24$$
$$\omega_4 = C22 - C23 - C24 - C25$$
$$\omega_5 = C23 - C24 - C25 - C26$$
$$\omega_6 = C23 - C24 - C25 - C27$$

where terminal methyls C26 and C27 are distinguished by viewing along the H2-C25 bond and following the clockwise sequence C24, C26, C27. Two additional dihedral angles will be defined here. The hydroxyl orientation is described by ω_0 (C2 – C3 – O—H1), and for an alternative description of the iso-octyl terminus, we consider ω_7 (C23 – C24 – C25 – H2). While rotations around these bonds could generate hundreds of conformers, Duax et al. found that the crystal structures indicate a set of six principal conformer types that are favoured. Type A represents a fully extended *trans* chain while types B, C, D_1, D_2 and D_3 have specific patterns of *trans* and *gauche* conformations for ω_2, ω_3 and ω_4. Within a conformer type, ω_5 and ω_6, take various *trans* and *gauche* values. In the present work, conformers were randomly generated, sorted by a low-level energy estimate and then further optimized by DFT. Raman calculations were carried out on the 10 conformers that are detailed in Table 1. The conformer types are based on the notation of Duax et al. but modified for the Raman results reported here.

The Raman spectra for conformers 2 (type A), 5 (type $D_{1,3}$) and 7 (type D_{2a}) were calculated from 200 to 1000 cm^{-1} and are plotted in the Supporting Material to show the level of variation in different spectral regions. Here we focus on the spectral band from 520 to 650 cm^{-1} (Figure 3) for all conformers in Table 1. Each spectrum contains six clear peaks in this band which represent the same six vibrations of the steroid rings with some minor contribution from stretching of bonds in the chain. The six peak positions and amplitudes shift based on the conformation of the iso-octyl chain. The 10 spectra in Figure 3 fall into four spectral types which correspond closely, but not exactly, to the conformer types defined by Duax et al. The spectra of the three type A all-*trans* conformers have uniformly spaced peaks. Conformer types

Research Article
doi.org/10.1002/ansa.202300057
Chemistry Europe
European Chemical Societies Publishing

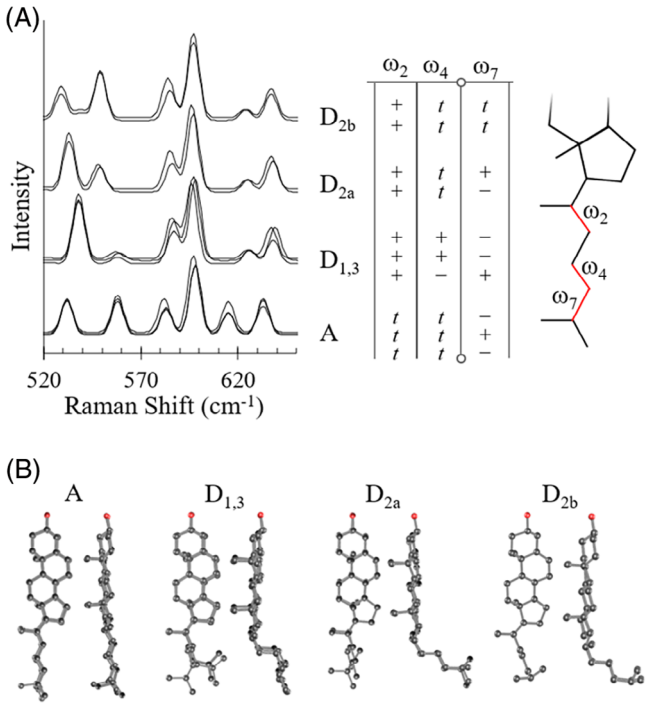

FIGURE 3 The Raman spectra of 10 conformers for the band sensitive to chain structure. The spectra are grouped into four spectral types and the dihedral angles are given in the adjacent table (A). The molecular structure highlights the bonds of interest. The cholesterol structures are drawn at two angles to illustrate the position of the chain relative to the steroid rings (B).

D_1 and D_3 are *gauche* for ω_2 and ω_4 and differ by the positive or negative *gauche* value for ω_7, but this does not affect the calculated Raman spectrum so the conformers are grouped and labelled $D_{1,3}$. Four of the calculated conformers fall under type D_2, but they have two distinct Raman spectra, so they are labelled D_{2a} and D_{2b}. The structural difference between them is in the chain terminus with ω_7 *gauche* for D_{2a} and *trans* for D_{2b}.

The structural significance of these spectral groups is illustrated with an adjacent table of dihedral angles in Figure 3A and the molecular structures drawn in Figure 3B. The bond rotations that impact the spectral group are at the second and fourth bonds of the chain (ω_2 and ω_4) and at the terminal structure (ω_7). Type A represents a straight chain and is the most common conformer found among crystal structures according to Duax et al. The $D_{1,3}$ types are *gauche* at ω_2 which directs the chain transverse to the plane of the rings, but another *gauche* bond for ω_4 minimizes the deviation. The D_2 types, which are *gauche* at ω_2 and *trans* at ω_4 show the greatest deviation from the plane of the rings.

3.3 | The iso-octyl chain structure

The modulation of cholesterol's ring vibrations by its chain conformation provides a new opportunity for structural analysis. The peak 10–15 bands of the Raman spectrum recorded from powdered microcrystalline cholesterol were fit to a linear combination of the four

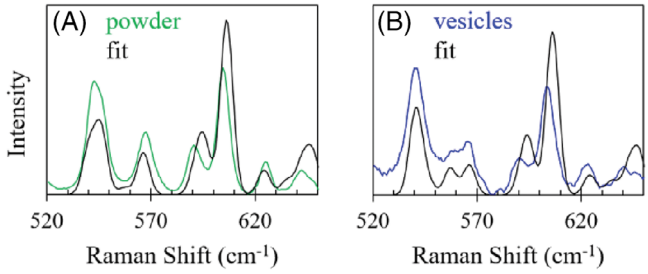

FIGURE 4 Fits of the calculated Raman spectra to measured spectra for powdered cholesterol (A) and cholesterol in phospholipid vesicles (B).

TABLE 2 The relative fractions of each set of cholesterol chain conformers for powder and vesicle samples. The brackets show the 95% confidence interval values.

Spectral type	Microcrystalline powder	Phospholipid vesicles
D_{2b}	0.00*	0.00*
D_{2a}	0.07 [−0.08, 0.22]	0.61 [0.41, 0.82]
$D_{1,3}$	0.48 [0.36, 0.61]	0.04 [−0.13, 0.20]
A	0.45 [0.32, 0.58]	0.35 [0.18, 0.52]

*The coefficient was held to zero by a constraint.

spectral types in Figure 3. The fit is presented in Figure 4A and the coefficients for the conformer types are in Table 2. According to the fit, the main contributions are from conformer types A (the straight *trans* chain) and $D_{1,3}$ (the chain with minimal deviation from the plane of the steroid rings). These results are consistent with reported crystal structures of cholesterol which have multiple conformers per unit cell, but largely in a straight *trans* structure.[70] The iso-octyl chain structure can also be analyzed for cholesterol in its more natural lipid bilayer state. Dioleoyl phosphatidylcholine (DOPC) vesicles were prepared with and without 30% cholesterol. The vesicle spectra were subtracted to isolate the cholesterol contribution. In lipid vesicles, 20 of the 23 peaks were observed (see Supporting Material). The band of peaks 10–15 was clearly detected, although some peaks were shifted and split compared to the powder spectrum, which is consistent with a different chain structure. The peak 10-15 band was fit to the four spectral types as above (Figure 4B) and the conformer distribution is in Table 2. In lipid vesicles, the chain structure shows a significant shift towards type D_{2a} at the expense of types A and $D_{1,3}$, representing an increase in conformers with chains bent perpendicular to the steroid rings.

The prevalence of cholesterol-conformer type D_{2a} in DOPC vesicles is consistent with cholesterol's condensing effect on disordered phospholipid membranes. The condensation effect was first observed for lipid monolayers at the air-water interface, where the addition of cholesterol lowered the area per lipid in the monolayer.[71] Cholesterol was later found to have a similar condensing effect on lipid bilayers, which impacts membrane flexibility and permeability.[72,73] Although the cholesterol condensation effect has been widely studied, the precise molecular mechanism is not yet known and several proposed models are still under investigation.[74] The effect is usually associated

with van der Waals interactions between phospholipid acyl chains and cholesterol's steroid rings, but recent nuclear magnetic resonance and molecular dynamics studies suggest that cholesterol's iso-octyl chain also plays an equally important role.[75,76] Vogel et al. found evidence that the chain dihedral angles take new values in lipids as compared to crystal structures.[77] Based on these angles, they conclude that the chain tends to move perpendicular to the plane of the rings in phospholipid membranes. Here we draw the same conclusion directly from the Raman vibrational spectra of the cholesterol molecule. In the DOPC membrane in which all phospholipid chains have a *cis* double bond, the cholesterol chain may reorient to fill free space and allow a tighter packing of the DOPC lipids. These results will be made more accurate and comprehensive with future work that will include more conformer calculations and measurements with different phospholipid species.

4 | CONCLUSION

Through a comparison of TDDFT-calculated Raman spectra with measurements on microcrystalline powder and solution phase vesicles, the detailed molecular motions corresponding to 23 peaks in cholesterol's Raman spectrum have been identified. A band of six peaks was found to have relative positions and intensities that depend on the conformation of the iso-octyl chain. By fitting the spectra of different conformers to experimental data, distributions of conformer structures were found. In phospholipid vesicles, the cholesterol chain was found to shift perpendicular to the plane of the fused rings, consistent with its role in phospholipid condensation. These results show that complex vibrations of molecules as large as cholesterol can be identified by TDDFT and, more importantly, that the vibrations contain useful and decipherable information on molecular structure and interactions despite the global molecular motions they represent.

AUTHOR CONTRIBUTIONS

Jason H. Hafner, Mathieu L. Simeral and Steven M. E. Demers designed the research, Mathieu L. Simeral, Steven M. E. Demers and Kyle Sheth performed the research, Mathieu L. Simeral and Jason H. Hafner contributed to analytic tools and Jason H. Hafner wrote the manuscript.

ACKNOWLEDGEMENTS

The authors gratefully acknowledge funding from the National Science Foundation award number 1709084 and the Welch Foundation under grant C-2140-20230405. This work was supported by the Office of the Assistant Secretary of Defense for Health Affairs and the Defense Health Agency J9, Research and Development Directorate, through the (Peer Reviewed Medical Research Program Discovery Award) under Award No. W81XWH-21-1-0002. Opinions, interpretations, conclusions, and recommendations are those of the author and are not necessarily endorsed by the Department of Defense.

CONFLICT OF INTEREST STATEMENT

The authors declare no conflicts of interest.

DATA AVAILABILITY STATEMENT

The data that support the findings of this study are available from the corresponding author upon reasonable request.

ORCID

Jason H. Hafner https://orcid.org/0000-0002-6943-4232

REFERENCES

1. Larkin P. *IR and Raman Spectroscopy*. Elsevier; 2011.
2. Handzo B, Peters J, Kalyanaraman R. A fingerprint in a fingerprint: a Raman spectral analysis of pharmaceutical ingredients. *Spectroscopy*. 2022;37(3):24-30.
3. Nasdala L, Schmidt C. Applications of Raman spectroscopy in mineralogy and geochemistry. *Elements*. 2020;16:99-104.
4. Osterhout JT, Schopf JW, Kudryavtsev AB, Czaja AD, Williford KH. Deep-UV Raman spectroscopy of carbonaceous Precambrian microfossils: insights into the search for past life on mars. *Astrobiology*. 2022;22:1239-1254.
5. Rull F, Veneranda M, Manrique-Martinez JA, et al. Spectroscopic study of terrestrial analogues to support rover missions to Mars—A Raman-centred review. *Anal Chim Acta*. 2021:339003.
6. Bordes L, Prinsloo LC, Fullagar R, Roberts RG. A key to identify use-related micro-residues on prehistoric stone artefacts using Raman spectroscopy. *J Archaeol Sci Rep*. 2020;31:102329.
7. Wang K, Li Z, Li J, Lin H. Raman spectroscopic techniques for nondestructive analysis of agri-foods: a state-of-the-art review. *Trends Food Sci Technol*. 2021;118:490-504.
8. Zhang CC, Hartlaub S, Petrovic I, Yilmaz B. Raman spectroscopy characterization of amorphous coke generated in industrial processes. *ACS Omega*. 2022;7:2565-2570.
9. Pezzotti G. Raman spectroscopy in cell biology and microbiology. *J Raman Spectrosc*. 2021;52:2348-2443.
10. Ralbovsky NM, Lednev IK. Towards development of a novel universal medical diagnostic method: Raman spectroscopy and machine learning. *Chem Soc Rev*. 2020;49:7428-7453.
11. Zini J, Saari H, Ciana P, et al. Infrared and Raman spectroscopy for purity assessment of extracellular vesicles. *Eur J Pharm Sci*. 2022;172:106135.
12. Daoust F, Nguyen T, Orsini P, et al. Handheld macroscopic Raman spectroscopy imaging instrument for machine-learning-based molecular tissue margins characterization. *J Biomed Opt*. 2021;26:022911.
13. Payne CM, Anderson LJE, Hafner JH. Novel plasmonic structures based on gold nanobelts. *J Phys Chem C*. 2013;117:4734-4739.
14. Pacia MZ, Czamara K, Zebala M, Kus E, Chlopicki S, Kaczor A. Rapid diagnostics of liver steatosis by Raman spectroscopy *via* fiber optic probe: a pilot study. *Analyst*. 2018;143:4723-4731.
15. Baenke F, Peck B, Miess H, Schulze A. Hooked on fat: the role of lipid synthesis in cancer metabolism and tumour development. *Dis Model Mech*. 2013;6:1353-1363.
16. Czamara K, Majzner K, Pacia MZ, Kochan K, Kaczor A, Baranska M. Raman spectroscopy of lipids: a review. *J Raman Spectrosc*. 2015;46:4-20.
17. Movasaghi Z, Rehman S, Rehman IU. Raman spectroscopy of biological tissues. *Appl Spectrosc Rev*. 2007;42:493-541.
18. Carney RP, Hazari S, Colquhoun M, et al. Multispectral optical tweezers for biochemical fingerprinting of CD9-positive exosome subpopulations. *Anal Chem*. 2017;89:5357-5363.
19. Smith ZJ, Lee C, Rojalin T, et al. Single exosome study reveals subpopulations distributed among cell lines with variability related to membrane content. *J Extracell Vesicles*. 2015;4:28533.
20. Liang H, Cheng X, Dong S, et al. Rapid and non-invasive discrimination of acute leukemia bone marrow supernatants by Raman

spectroscopy and multivariate statistical analysis. *J Pharm Biomed Anal*. 2022;210:114560.
21. Alfonso-García A, Pfisterer SG, Riezman H, Ikonen E, Potma EO. D38-cholesterol as a Raman active probe for imaging intracellular cholesterol storage. *J Biomed Opt*. 2015;21:061003.
22. Yue S, Li J, Lee S-Y, et al. Cholesteryl ester accumulation induced by PTEN loss and PI3K/AKT activation underlies human prostate cancer aggressiveness. *Cell Metab*. 2014;19:393-406.
23. van Manen H-J, Otto C. Cholesterol esters are detected by Raman microspectroscopy in HeLa cells. *J Raman Spectrosc*. 2009;40:117-118.
24. Hawi SR, Nithipatikom K, Wohlfeil ER, Adar F, Campbell WB. Raman microspectroscopy of intracellular cholesterol crystals in cultured bovine coronary artery endothelial cells. *J Lipid Res*. 1997;38:1591-1597.
25. Shirota K, Yagi K, Inaba T, et al. Detection of sphingomyelin clusters by Raman spectroscopy. *Biophys J*. 2016;111:999-1007.
26. Ando J, Kinoshita M, Cui J, et al. Sphingomyelin distribution in lipid rafts of artificial monolayer membranes visualized by Raman microscopy. *Proc Natl Acad Sci*. 2015;112:4558-4563.
27. Okotrub KA, Zaytseva IV, Adichtchev SV, Surovtsev NV. Raman spectroscopy and DSC assay of the phase coexistence in binary DMPC/cholesterol multilamellar vesicles. *Biochim Biophys Acta Biomembr*. 2021;1863:183514.
28. Genova J, Petrov M, Bivas I, Rafailov P, Naradikian H, Katranchev B. Fourier-transform infrared and Raman characterization of bilayer membranes of the phospholipid SOPC and its mixtures with cholesterol. *Colloids Surf Physicochem Eng Asp*. 2018;557:85-93.
29. Ikonen E. Cellular cholesterol trafficking and compartmentalization. *Nat Rev Mol Cell Biol*. 2008;9:125-138.
30. Chakraborty S, Doktorova M, Molugu TR, et al. How cholesterol stiffens unsaturated lipid membranes. *Proc Natl Acad Sci*. 2020;117:21896-21905.
31. Alwarawrah M, Dai J, Huang J. A molecular view of the cholesterol condensing effect in DOPC lipid bilayers. *J Phys Chem B*. 2010;114:7516-7523.
32. Elkins MR, Bandara A, Pantelopulos GA, Straub JE, Hong M. Direct observation of cholesterol dimers and tetramers in lipid bilayers. *J Phys Chem B*. 2021;125:1825-1837.
33. Pantelopulos GA, Straub JE. Regimes of complex lipid bilayer phases induced by cholesterol concentration in MD simulation. *Biophys J*. 2018;115:2167-2178.
34. Kanmalar M, Abdul Sani SF, Kamri N, et al. Raman spectroscopy biochemical characterisation of bladder cancer cisplatin resistance regulated by FDFT1: a review. *Cell Mol Biol Lett*. 2022;27:9.
35. Silveira L, de CF Borges R, Navarro RS, et al. Quantifying glucose and lipid components in human serum by Raman spectroscopy and multivariate statistics. *Lasers Med Sci*. 2017;32:787-795.
36. Lee HJ, Zhang W, Zhang D, et al. Assessing cholesterol storage in live cells and C. elegans by stimulated Raman scattering imaging of phenyldiyne cholesterol. *Sci Rep*. 2015;5:7930.
37. Tripp M, Wiemann J, Brocks J, Mayer P, Schwark L, Grice K. Fossil biomarkers and biosignatures preserved in coprolites reveal carnivorous diets in the carboniferous Mazon Creek ecosystem. *Biology*. 2022;11:1289.
38. Velde G, Bickelhaupt FM, Baerends EJ, et al. Chemistry with ADF. *J Comput Chem*. 2001;22:931-967.
39. Neugebauer J, Reiher M, Kind C, Hess BA. Quantum chemical calculation of vibrational spectra of large molecules—Raman and IR spectra for Buckminsterfullerene. *J Comput Chem*. 2002;23:895-910.
40. Pérez-Jiménez AI, Lyu D, Lu Z, Liu G, Ren B. Surface-enhanced Raman spectroscopy: benefits, trade-offs and future developments. *Chem Sci*. 2020;11:4563-4577.
41. Bell SEJ, Charron G, Cortés E, et al. Towards reliable and quantitative surface-enhanced Raman scattering (SERS): from key parameters to good analytical practice. *Angew Chem Int Ed*. 2020;59:5454-5462.
42. McNay G, Eustace D, Smith WE, Faulds K, Graham D. Surface-enhanced Raman scattering (SERS) and surface-enhanced resonance Raman scattering (SERRS): a review of applications. *Appl Spectrosc*. 2011;65:825-837.
43. Smith WE. Practical understanding and use of surface enhanced Raman scattering/surface enhanced resonance Raman scattering in chemical and biological analysis. *Chem Soc Rev*. 2008;37:955-964.
44. Jensen L, Schatz GC. Resonance Raman scattering of rhodamine 6G as calculated using time-dependent density functional theory. *J Phys Chem A*. 2006;110:5973-5977.
45. van Gisbergen SJA, Snijders JG, Baerends EJ. Application of time-dependent density functional response theory to Raman scattering. *Chem Phys Lett*. 1996;259:599-604.
46. Simeral ML, Hafner JH. The Raman active vibration modes of the anthraquinones. *Astrobiology*. 2022;22:1165-1175.
47. Uyeki CM, Pacheco CM, Simeral ML, Hafner JH. The Raman active vibrations of flavone and quercetin: the impact of conformers and hydrogen bonding on fingerprint modes. *J Phys Chem A*. 2023;127:1387-1394.
48. Fonseca Guerra C, Snijders JG, te Velde G, Baerends EJ. Towards an order-N DFT method. *Theor Chem Acc*. 1998;99:391-403.
49. van Lenthe E, Baerends EJ. Optimized Slater-type basis sets for the elements 1-118. *J Comput Chem*. 2003;24:1142-1156.
50. van Lenthe E, Ehlers A, Baerends E-J. Geometry optimizations in the zero order regular approximation for relativistic effects. *J Chem Phys*. 1999;110:8943-8953.
51. van Lenthe E, Baerends EJ, Snijders JG. Relativistic regular two-component Hamiltonians. *J Chem Phys*. 1993;99:4597-4610.
52. van Lenthe E, Baerends EJ, Snijders JG. Relativistic total energy using regular approximations. *J Chem Phys*. 1994;101:9783-9792.
53. Fan L, Ziegler T. Application of density functional theory to infrared absorption intensity calculations on transition-metal carbonyls. *J Phys Chem*. 1992;96:6937-6941.
54. Fan L, Ziegler T. Application of density functional theory to infrared absorption intensity calculations on main group molecules. *J Chem Phys*. 1992;96:9005-9012.
55. van Gisbergen SJA, Snijders JG, Baerends EJ. A density functional theory study of frequency-dependent polarizabilities and Van der Waals dispersion coefficients for polyatomic molecules. *J Chem Phys*. 1995;103:9347-9354.
56. van Gisbergen SJA, Snijders JG, Baerends EJ. Implementation of time-dependent density functional response equations. *Comput Phys Commun*. 1999;118:119-138.
57. Jensen L, Autschbach J, Krykunov M, Schatz GC. Resonance vibrational Raman optical activity: a time-dependent density functional theory approach. *J Chem Phys*. 2007;127:134101.
58. Lippert JL, Peticolas WL. Laser Raman investigation of the effect of cholesterol on conformational changes in dipalmitoyl lecithin multilayers. *Proc Natl Acad Sci*. 1971;68:1572-1576.
59. Mendelsohn R. Laser-Raman spectroscopic study of egg lecithin and egg lecithin-cholesterol mixtures. *Biochim Biophys Acta Biomembr*. 1972;290:15-21.
60. Faiman R. Raman spectroscopic studies of different forms of cholesterol and its derivatives in the crystalline state. *Chem Phys Lipids*. 1977;18:84-104.
61. Wallach DFH, Verma SP, Fookson J. Application of laser Raman and infrared spectroscopy to the analysis of membrane structure. *Biochim Biophys Acta Rev Biomembr*. 1979;559:153-208.
62. Pink DA, Green TJ, Chapman D. Raman scattering in bilayers of saturated phosphatidylcholines and cholesterol. Experiment and theory. *Biochemistry*. 1981;20:6692-6698.
63. Kalkura SN, Ramakrishnan V, Devanarayanan S. IR and Raman studies of cholesterol monohydrate grown in gel medium. *Infrared Phys*. 1987;27:335-337.

64. Le Cacheux P, Menard G, Quang HN, Weinmann P, Jouan M, Dao NQ. Quantitative analysis of cholesterol and cholesterol ester mixtures using near-infrared Fourier transform Raman spectroscopy. *Appl Spectrosc*. 1996;50:1253-1257.
65. Simeral ML, Zhang A, Demers SME et al. Effects of conformational variation on structural insights from solution-phase surface-enhanced Raman spectroscopy. *J Phys Chem B*. 2021;125:2031-2041.
66. Ebejer J-P, Morris GM, Deane CM. Freely available conformer generation methods: how good are they? *J Chem Inf Model*. 2012;52:1146-1158.
67. Kesharwani MK, Brauer B, Martin JML. Frequency and zero-point vibrational energy scale factors for double-hybrid density functionals (and other selected methods): can anharmonic force fields be avoided? *J Phys Chem A*. 2015;119:1701-1714.
68. Laury ML, Carlson MJ, Wilson AK. Vibrational frequency scale factors for density functional theory and the polarization consistent basis sets. *J Comput Chem*. 2012;33:2380-2387.
69. Duax WL, Griffin JF, Rohrer DC, Weeks CM. Conformational analysis of sterols: comparison of X-ray crystallographic observations with data from other sources. *Lipids*. 1980;15:783-792.
70. Shieh H-S, Hoard LG, Nordman CE. The structure of cholesterol. *Acta Crystallogr B*. 1981;37:1538-1543.
71. Leathes JB. On the role of fats in vital phenomena. *Lancet*. 1925;205:853-856.
72. Yeagle PL. Cholesterol and the cell membrane. *Biochim Biophys Acta Rev Biomembr*. 1985;822:267-287.
73. Ohvo-Rekilä H, Ramstedt B, Leppimäki P, Peter Slotte J. Cholesterol interactions with phospholipids in membranes. *Prog Lipid Res*. 2002;41:66-97.
74. Regen SL. Cholesterol's condensing effect: unpacking a century-old mystery. *JACS Au*. 2022;2:84-91.
75. Scheidt HA, Meyer T, Nikolaus J et al. Cholesterol's aliphatic side chain modulates membrane properties. *Angew Chem Int Ed*. 2013;52:12848-12851.
76. Robalo JR, Ramalho JPP, Huster D, Loura LMS. Influence of the sterol aliphatic side chain on membrane properties: a molecular dynamics study. *Phys Chem Chem Phys*. 2015;17:22736-22748.
77. Vogel A, Scheidt HA, Jae Baek D, Bittman R, Huster D. Structure and dynamics of the aliphatic cholesterol side chain in membranes as studied by 2 H NMR spectroscopy and molecular dynamics simulation. *Phys Chem Chem Phys*. 2016;18:3730-3738.

SUPPORTING INFORMATION

Additional supporting information can be found online in the Supporting Information section at the end of this article.

How to cite this article: Simeral ML, Demers SME, Sheth K, Hafner JH. A Raman spectral marker for the iso-octyl chain structure of cholesterol. *Anal Sci Adv*. 2024;5:2300057. https://doi.org/10.1002/ansa.202300057